JACS
JOURNAL OF THE AMERICAN CHEMICAL SOCIETY

ARTICLE

pubs.acs.org/JACS

Ejection of Solvated Ions from Electrosprayed Methanol/Water Nanodroplets Studied by Molecular Dynamics Simulations

Elias Ahadi and Lars Konermann*

Department of Chemistry, The University of Western Ontario, London, Ontario N6A 5B7, Canada

Supporting Information

ABSTRACT: The ejection of solvated small ions from nanometer-sized droplets plays a central role during electrospray ionization (ESI). Molecular dynamics (MD) simulations can provide insights into the nanodroplet behavior. Earlier MD studies have largely focused on aqueous systems, whereas most practical ESI applications involve the use of organic cosolvents. We conduct simulations on mixed water/methanol droplets that carry excess NH_4^+ ions. Methanol is found to compromise the H-bonding network, resulting in greatly increased rates of ion ejection and solvent evaporation. Considerable differences in the water and methanol escape rates cause time-dependent changes in droplet composition. Segregation occurs at low methanol concentration, such that layered droplets with a methanol-enriched periphery are formed. This phenomenon will enhance the partitioning of analyte molecules, with possible implications for their ESI efficiencies. Solvated ions are ejected from the tip of surface protrusions. Solvent bridging prior to ion secession is more extensive for methanol/water droplets than for purely aqueous systems. The ejection of solvated NH_4^+ is visualized as diffusion-mediated escape from a metastable basin. The process involves thermally activated crossing of a ~30 kJ mol^{-1} free energy barrier, in close agreement with the predictions of the classical ion evaporation model.

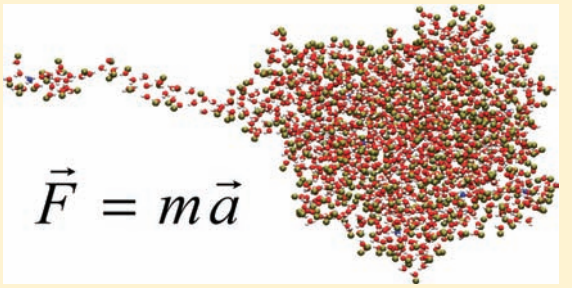

INTRODUCTION

Ever since Rayleigh's seminal studies in the late 1800s,[1] electrically charged solvent droplets have been the subject of experimental and theoretical investigations. Recent work has focused on these systems from an electrospray ionization (ESI) perspective,[2−15] although charged droplets also play an important role in atmospheric chemistry. ESI represents one of the most commonly used ionization methods for mass spectrometry (MS),[16] and it allows the transfer of a wide range of analytes from solution into the gas phase. During ESI, droplets of analyte solution are emitted from the tip of a Taylor cone. For typical infusion rates of a few microliters per minute, the radii of the initially formed droplets are in the micrometer range.[17] In positive ion mode, the droplets carry excess charge due to the presence of cationic species such as protons, sodium, or ammonium ions. Solvent evaporation reduces the droplet size to a point where cohesive interactions are balanced by electrostatic repulsion. At this so-called Rayleigh limit, the net charge Q_R is given by[1,2]

$$Q_R = 8\pi(\varepsilon_0 \gamma {r_0}^3)^{1/2} \quad (1)$$

where r_0 is the droplet radius, ε_0 is the permittivity of the vacuum, and γ is the surface tension. Droplets close to the Rayleigh limit can distort into nonspherical shapes with Taylor cone-like surface protrusions. This is followed by jet emission of smaller but highly charged progeny droplets from the protrusion tips.[2,18,19] Droplet fission events of this type may occur as thermally activated processes even slightly below Q_R. The significance of eq 1 is that the activation barrier height becomes zero at the Rayleigh limit, such that certain types of droplet disintegration events can proceed in an energetic downhill fashion.[1,19−21] Repeated evaporation/fission events ultimately lead to nanometer-sized droplets from which analyte molecules are released as intact gas phase ions.

The final steps of the ESI process are still a matter of debate, and two limiting scenarios are usually discussed in the literature. Large gas phase analyte ions such as proteins are likely formed by the charged residue mechanism (CRM), first proposed by Dole.[22] According to this scenario, the final ESI nanodroplets are just slightly larger than the macromolecular species contained within them. Free gas phase ions are formed by evaporation to dryness, concomitant with transfer of most of the droplet charge to the analyte.[2,23] Experimental support for the CRM comes from the fact that the ESI charge states of globular proteins match the Q_R value (eq 1) expected for water droplets of the same size.[24−28] Also, the formation of salt clusters[29] and nonspecific adducts[30−32] during ESI has been interpreted as evidence in favor of the CRM.

Very small analyte ions are thought to be formed via the ion evaporation mechanism (IEM), a framework developed by Iribarne and Thomson[33,34] and subsequently expanded by others.[35−38] Most investigations related to the IEM have focused on the generation of gas phase species such as Na^+ and NH_4^+ that exist as preformed ions in solution. The early events of solvent evaporation and droplet fission are the same as for the CRM. However, once a critical droplet

Received: December 21, 2010
Published: May 18, 2011

dx.doi.org/10.1021/ja111492s | J. Am. Chem. Soc. 2011, 133, 9354–9363

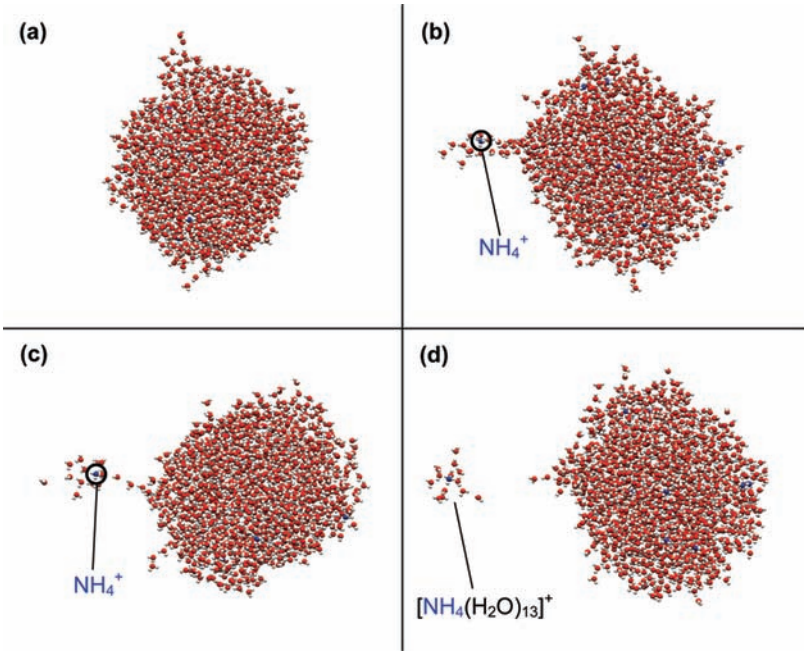

Figure 1. Snapshots taken from a MD trajectory of a nanodroplet initially containing 1500 water molecules and 11 ammonium ions. Hydrogen atoms are shown in white, oxygen in red, and nitrogen in blue. The time points shown correspond to (a) $t = 0$ ps, (b) $t = 207$ ps, (c) $t = 212$ ps, and (d) $t = 219$ ps. The location of the ammonium ion that is poised to be emitted is indicated in panels (b) and (c). Also indicated in (d) is the overall composition of the ejected cluster.

radius of a few nanometers is reached, the IEM stipulates that the electric field at the droplet surface becomes sufficiently high to allow the ejection of solvated charge carriers into the vapor phase.[2,15,33,36,37] Transition state theory has been applied to express the first-order rate constant k of these field emission events as[33,36,37,39]

$$k = \frac{k_B T}{h} \exp\left(\frac{-\Delta G^*}{k_B T}\right) \qquad (2)$$

where ΔG^* represents the height of the activation free energy barrier, k_B is the Boltzmann constant, h is Planck's constant, and T is the temperature.

The distinction between CRM and IEM on the basis of analyte size remains a matter of debate.[39,40] Some researchers propose that the IEM is operative even for proteins and other large analytes.[41,42] It has also been noted that protein charge states do not always follow the surface tension dependence that is expected for the CRM (eq 1).[43] Proposals of hybrid mechanisms have been put forward that involve elements of both the CRM and the IEM.[13]

The difficulties in arriving at a comprehensive understanding of the ESI process are related to the fact that nanometer-sized droplets occupy a size regime that is difficult to access experimentally. Insights into the behavior of much larger (early) ESI droplets come from phase Doppler interferometry[44] and from various imaging techniques.[45−48] At the other end of the size spectrum, small clusters containing only a few dozen solvent molecules can be interrogated by infrared spectroscopy[49−51] and by direct mass analyses.[52] Late ESI droplets, however, contain on the order of a few thousand solvent molecules which makes them challenging targets for those experimental techniques.

Molecular dynamics (MD) simulations represent an interesting approach for gaining insights into the behavior of nanometer-sized droplets.[10,11,14,53−59] For example, Znamenskiy et al.[53] used this approach for studying the ejection of solvated low molecular weight ions. It was found that ion emission occurs from the tip of transient solvent protrusions, resembling asymmetric droplet fission events seen in experiments on much larger systems.[45,46,48] Another recent study explored the location of charge carriers within ESI droplets. Much of the ESI literature implies that excess ions should be located directly at the solvent/vapor interface, as predicted by continuum electrostatic considerations.[1,2,23,41] This view is in apparent conflict with the tendency of ions such as Na^+ to migrate toward the interior where solvation is more favorable,[54,60] a point that was already raised in the initial IEM paper.[33] MD simulations reconciled the two viewpoints by demonstrating that small atomic cations do indeed reside within the droplet, but that all of the excess charge is projected to the outermost solvent layers by dipole-mediated polarization effects.[61]

The current work employs MD simulations for gaining better insights into the structure and dynamics of nanometer-sized (late) ESI droplets at the Rayleigh limit, with particular focus on the mechanism of charge carrier ejection ("ion evaporation"). Most previous ESI modeling studies focused on aqueous systems, whereas mixed aqueous/organic droplets have been explored to a much lesser extent. Yet, organic cosolvents such as methanol are of major importance for reversed-phase chromatographic analyses and many other ESI-MS applications.[6] The current work closes this gap by exploring the behavior of methanol/water droplets. We demonstrate the occurrence of solvent segregation and differential evaporation. Ammonium ions are chosen as charge carriers, reflecting the prevalence of NH_4^+ in many ESI-MS solvent systems.[2,6] While the droplets studied here do not contain any actual analyte molecules, the ejection of small cationic bioorganic species (e.g., drug molecules and metabolites) likely follows a field emission mechanism similar to that seen for NH_4^+.

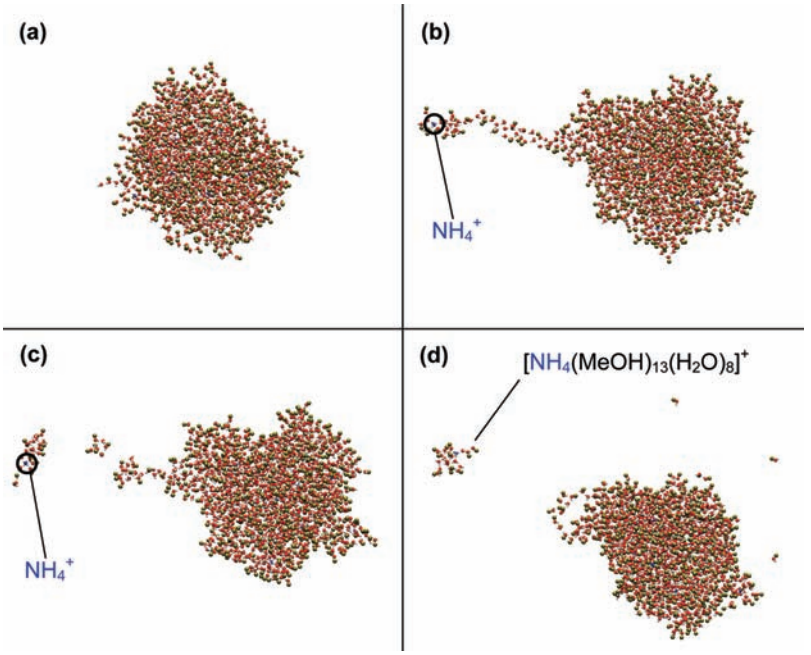

Figure 2. Snapshots taken from a MD trajectory of a nanodroplet initially containing 750 water, 750 methanol molecules, and 11 ammonium ions. Color coding is as in Figure 1, with methyl groups shown in ochre. Time points: (a) t = 0 ps, (b) t = 802 ps, (c) t = 816 ps, and (d) t = 845 ps.

METHODS

MD simulations on charged nanodroplets were carried out based on C++ code developed in-house, similar to that used for earlier studies from our laboratory.[60,61] Each droplet initially contained 1500 solvent molecules and 11 NH_4^+ ions. Five different water/methanol number ratios were tested, 100:0, 75:25, 50:50, 25:75, and 0:100. All simulations were carried out in a vacuum environment without imposing boundary conditions. The temporal evolution of the systems was simulated by integrating Newton's equations of motion using the Verlet algorithm[62,63] with a time step of 2 fs. The classical SPCE/E model was employed for water, with an O−H bond distance of 1.0 Å and a H−O−H angle of 109.47°.[64] Methanol was modeled using the H1 framework[65] where the $-CH_3$ group (Me) is treated as a single Lennard-Jones particle. In the H1 model the distances are 0.9451 Å for the O−H bond and 1.4246 Å for the Me−O bond. The Me−O−H angle is 108.53°. A N−H bond distance of 1.02 Å and a H−N−H angle of 109.47° was used for ammonium ions.[66] All bond lengths and angles were constrained using the SHAKE algorithm.[67] The solvent mixtures were initially subjected to Nose-Hoover thermalization[68,69] at 320 K for 100 ps. The simulations were then switched to constant energy MD (at $T \approx 320$ K) for 1 ns, during which particle coordinates were extracted every 0.4 ps for analysis. Three to six independent trajectories were calculated for each solvent composition. The onset of the constant energy runs is referred to as t = 0 time point. Lennard-Jones (LJ) parameters for water are σ_{OO} = 3.166 Å and ε_{OO} = 0.6502 kJ mol^{-1}, with charges $q_O = -0.8476e$ and $q_H = 0.4238e$.[64] LJ parameters for methanol are σ_{OO} = 3.083 Å and ε_{OO} = 0.7308 kJ mol^{-1}, σ_{MeMe} = 3.861 Å and ε_{MeMe} = 0.7575 kJ mol^{-1}, with charges $q_O = -0.728e$, $q_{Me} = 0.297e$ and $q_H = 0.431e$.[65] LJ parameters for ammonium ions are σ_{NN} = 3.45 Å and ε_{NN} = 0.7782 kJ mol^{-1}, with charges $q_N = -0.8172e$ and $q_H = 0.4543e$.[66] Mixing of these LJ parameters was performed according to $\sigma_{ij} = 0.5 \times (\sigma_{ii} + \sigma_{jj})$ and $\varepsilon_{ij} = (\varepsilon_{ii}\varepsilon_{jj})^{0.5}$.[70] Interactions between the hydrogen atoms of all three species were described purely based on the Coulomb potential. LJ potentials were truncated at 9.5 Å, whereas no cut-offs were employed for electrostatic interactions.[14] Electronic polarization effects have been shown to be quite important for modeling the behavior of large polarizable anions such as I^- and Br^-. In comparison, these effects are almost negligible for small cations of the type studied here.[54,71−78] Electronic polarization was thus not explicitly considered in this work, thereby simplifying the calculations and data analysis.[61] Radial distributions represent histograms that are plotted versus distance r from the droplet center of mass, corrected for the $4\pi r^2$ surface area of individual bins to account for the spherical geometry. H-bonds were identified by employing the geometric criterion that the O−O distance has to be less than 3.5 Å, and simultaneously the angle between the O−O axis and one of the O−H covalent bonds has to be less than 35°.[79] This method was applied to all three types of H-bonds: water−water, water−methanol, and methanol−methanol. Solvent molecules were considered to be evaporated from the droplet when their distance from the overall center of mass was more than 35 Å. Simulations were run on SHARCNET (www.sharcnet.ca). Desktop computers were used for smaller test systems, code development, and trajectory analyses. Images of MD frames were rendered using VMD.[80] Sigmaplot 11 was employed for least-squares fitting.

RESULTS AND DISCUSSION

Overall Droplet Behavior. MD simulations on charged nanodroplets containing 1500 solvent molecules were carried out for various water/methanol compositions, including pure water and pure methanol. At t = 0 ns, all systems exhibit a roughly spherical shape with some surface undulations (Figures 1a, 2a, 3a). Each of the droplets initially contained 11 NH_4^+ ions. Methanol and mixed water/methanol droplets are highly dynamic with relatively pronounced shape fluctuations during the simulation time window, numerous solvent evaporation events, and ejection of solvated ions (Figures 2 and 3). In contrast, purely aqueous droplets maintain a more spherical geometry (Figure 1), solvent evaporation is less pronounced, and ion ejection is rare. All of these aspects will be discussed in more detail below.

The excess charge $Q = 11 \times 1.6 \times 10^{-19}$ C in our simulations was chosen to ensure that the initial droplets are close to the

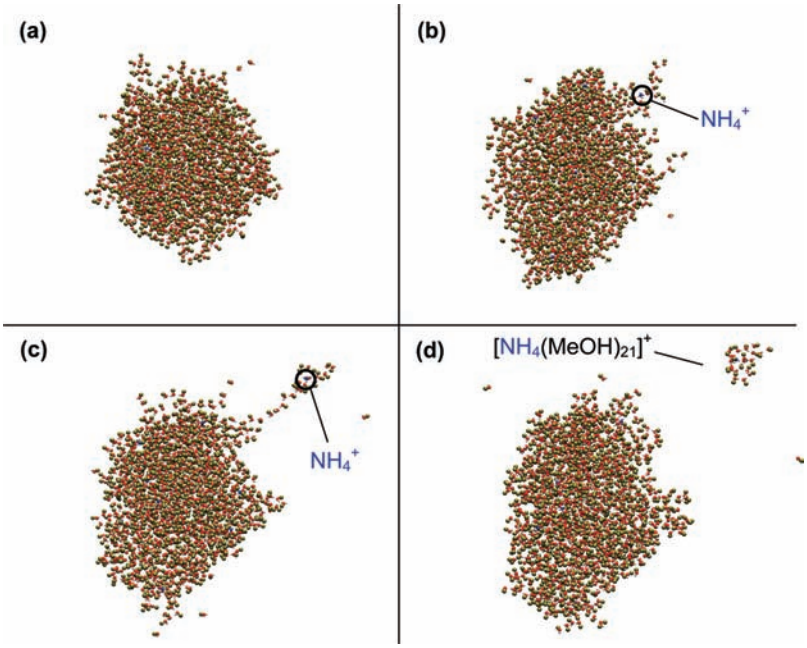

Figure 3. Snapshots taken from a MD trajectory of a nanodroplet initially containing 1500 methanol molecules and 11 ammonium ions. Color coding is as in Figures 1 and 2. The time points shown correspond to (a) t = 0 ps, (b) t = 572 ps, (c) t = 645 ps, and (d) t = 663 ps.

Rayleigh limit (eq 1), mimicking the size and charge regime encountered during the final stages of the ESI process.[2,81] Calculating the ratio Q/Q_R requires the droplet radii r_0 to be determined. Consistent with earlier results,[53,54] the liquid/vapor boundary of the simulated systems is relatively diffuse, with sigmoidal transitions in the corresponding solvent radial distribution functions (Figure 4). r_0 values were estimated from the midpoints of these transitions,[61] resulting in $r_0 \approx 21$ Å for pure water (Figure 4a) and $r_0 \approx 28$ Å for pure methanol (Figure 4e). Values for mixed water/methanol systems fall in-between these two numbers. These data reflect the bulkier nature of the methyl group in CH_3-OH relative to hydrogen in H−OH. The tabulated surface tension values γ of pure water and methanol are 0.0720 and 0.0225 N m^{-1}, respectively.[82] These bulk values are quite well reproduced by solvent models of the type used here.[83,84] From eq 1 it follows that the charge on our aqueous droplets corresponds to $Q/Q_R = 0.91$, whereas the value for pure methanol is 1.06. We reiterate that the formation of these systems under experimental conditions starts with much larger droplets, which then undergo repeated cycles of evaporation and fission (see Introduction).[81] Those earlier ESI steps are not accessible by MD simulations. Instead, this work deals with charged nanodroplets that represent the penultimate stage en route to the release of analyte ions into the gas phase.[81]

Figure 1 depicts snapshots for the ejection of a solvated ammonium ion from a purely aqueous droplet. Formation of a surface protrusion that encloses a NH_4^+ ion (Figure 1b) is followed by a "bridged" arrangement where the departing cluster is connected to the parent droplet by a few H-bonded water molecules (Figure 1c). Subsequently, the solvent bridge collapses, and the charged cluster is Coulombically propelled away from the residual droplet (Figure 1d). Qualitatively similar observations have been reported in previous MD studies.[10,11,53,54,56,57]

Formation of a transient solvent bridge between the departing charged cluster and the parent droplet is more extensive for methanol-containing droplets than for purely aqueous systems. Figure 2b shows a 50:50 system where a very long (∼ 50 Å) protrusion involving both water and methanol has formed at the droplet surface. The gradual extension of this bridge is facilitated by electrostatic repulsion between the droplet and the solvated NH_4^+ at the protruding tip, up to a point where the bridge collapses (Figure 2c). The torn bridge elements then coalesce with the residual droplet, while the ejected cluster moves away from the center of mass (Figure 2d). A sequence of snapshots for an NH_4^+ emission event from a pure methanol droplet is depicted in Figure 3. The extent of bridging prior to secession (Figure 3c) is more pronounced than for the aqueous system (Figure 1c), but less than for the mixed cluster (Figure 2b). MD movies corresponding to Figures 1−3 can be found in the Supporting Information. The number of solvent molecules attached to the ejected ammonium ions is around 10−20 for the various conditions studied here. Somewhat smaller solvation numbers (up to 8 H_2O per NH_4^+) have been found experimentally.[34] However, it is likely that those experiments involve additional solvent evaporation prior to detection, such that our results do not contradict those of ref 34.

Earlier MD work has explored the surface energy S of nanometer-sized droplets.[83,85] S represents the product of γ and surface area. It is instructive to consider the magnitude of ΔS associated with ejection of solvated ions. ΔS may be estimated as the difference in potential energy of the solvent before and after ejection.[84] We will focus on aqueous droplets (Figure 1), for which the overall potential energy has contributions from H_2O/H_2O, H_2O/NH_4^+, and NH_4^+/NH_4^+ interactions. The H_2O/H_2O contribution is dominant, amounting to −60 400 kJ mol^{-1}. The others are −7700 and +3600 kJ mol^{-1}, respectively, with thermal fluctuations on the order of ±1%. Dividing the H_2O/H_2O component by the number of solvent molecules yields −60 400 kJ mol^{-1}/1500 = −40.3 kJ mol^{-1}. This is close to the experimental enthalpy of condensation ($-\Delta_{vap}H$),[82] −43 kJ mol^{-1}, thus, supporting the fidelity of our model. Ejection of a solvated ion from an aqueous nanodroplet (Figure 1) leads to a decrease in the overall

dx.doi.org/10.1021/ja111492s |J. Am. Chem. Soc. 2011, 133, 9354–9363

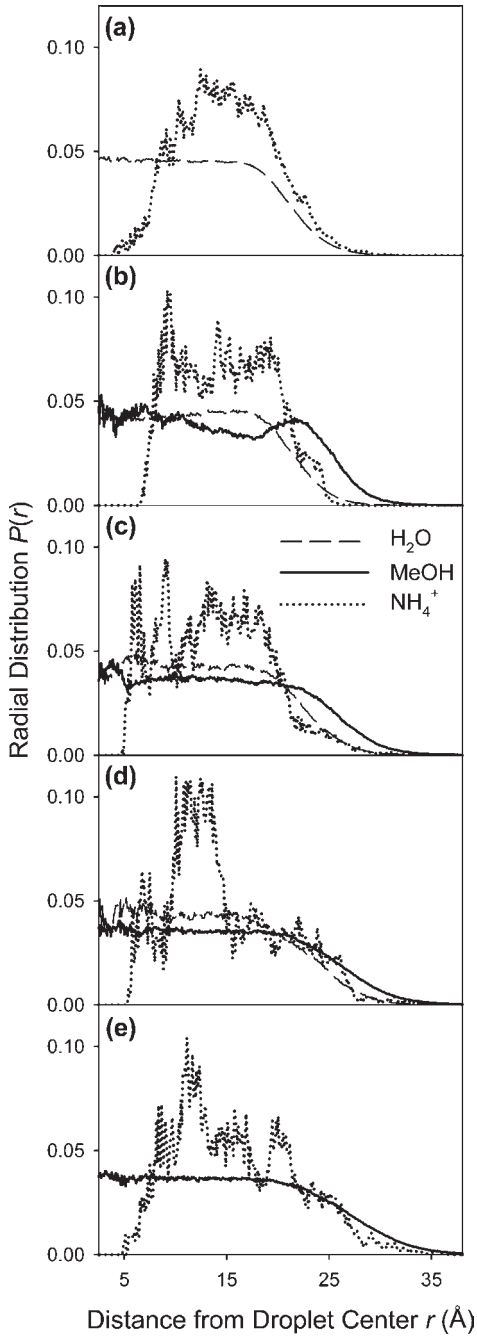

Figure 4. Radial distributions $P(r)$ for nanodroplets consisting of (a) 100% water, (b) 75% water/25% methanol, (c) 50% water/50% methanol, (d) 25% water/75% methanol, and (e) 100% methanol. Dashed lines, oxygen of water; solid lines, methyl group of methanol; dotted lines, nitrogen of NH_4^+. Data were averaged over the first 200 ps of four 1 ns simulations for each panel.

NH_4^+/NH_4^+ interaction energy. However, only the H_2O/H_2O and H_2O/NH_4^+ contributions are pertinent for determining ΔS. Both of these remain virtually unchanged during ejection (data not shown), such that ΔS is exceedingly small. More specifically, based on the limited number of water molecules involved (~15, Figure 1b), it can be stated that ΔS will not exceed 15/1500 = 1%. ΔS may be larger for the methanol-containing droplets due to the greater number of solvent molecules that participate in ion ejection (e.g., Figure 2b). Unfortunately, energetic analyses of those situations are complicated by extensive solvent evaporation throughout the droplet lifetime (see below).

Droplet Structure. Distribution functions $P(r)$ were generated by tallying the radial position r of all droplet constituents into normalized histograms (Figure 4). This procedure was restricted to the first 200 ps of each trajectory for minimizing the effects of shape fluctuations and solvent evaporation. An overall trend toward larger r_0 with increasing methanol concentration has already been discussed above. It is interesting to note demixing of the two solvents, where methanol preferentially adopts positions more in the droplet periphery. This segregation is most pronounced for systems containing 25% methanol (Figure 4b), whereas the effect is diminished at higher concentrations (Figure 4c,d). Enrichment of methanol at the liquid/vapor interface has previously been observed in simulations of planar systems,[86] and for small neutral clusters.[87] Consistent with our data (Figure 4), those previous studies[86,87] reported that demixing is most pronounced at low methanol concentrations. Microimmiscibilities were also found in MD studies and experimental investigations[88,89] on bulk water/methanol solutions.[90] Notably, none of those earlier studies[86−90] explored the behavior of highly charged systems. Our results confirm that segregation also occurs for methanol/water droplets that are close to the Rayleigh limit. The surface enrichment of methanol seen in Figure 4 confirms the intuitive expectation that favorable water−water interactions (through H-bonding, see next section) can be maximized by preferentially gathering H_2O molecules in the center of the droplet. At the same time, methanol with its mildly hydrophobic $-CH_3$ group exhibits a higher affinity for the droplet surface, a phenomenon that is reminiscent of the behavior expected for partially nonpolar ESI analytes.[6,91,92]

Similar to other cations,[53,54] NH_4^+ preferentially adopts radial positions toward the droplet interior, instead of being located at the solvent/vapor interface (dotted lines in Figure 4). This behavior is attributable to the more favorable solvation away from the surface, as mentioned in the Introduction and discussed in detail elsewhere.[61] Pure water droplets exhibit a simple bell-shaped $P(r)$ distribution for NH_4^+ (Figure 4a). In contrast, the NH_4^+ $P(r)$ profiles for methanol-containing droplets are more complex, reminiscent of data previously observed for other charge carriers.[53]

Hydrogen Bonding and Solvent Evaporation. H-bonding is the main cohesive interaction for both water and methanol, whereas van der Waals interactions (modeled as LJ potentials) play a lesser role. In bulk water, each molecule can donate ~2 H-bonds while also accepting ~2 H-bonds. In comparison, the propensity of methanol to act as donor and acceptor is compromised by the methyl group, resulting in less extensive H-bonding.[93] This behavior is reflected in the bulk vapor pressure values of 3.2 and 16.9 kPa for water and methanol, respectively, at 25 °C.[82]

As expected, the total number of H-bonds is highest for purely aqueous droplets. The 1500 waters form ~2700 interactions, corresponding to (2 × 2700)/1500 = 3.6 H-bonds per H_2O molecule. Addition of methanol gradually lowers the total number of H-bonds down to ~1300 for droplets that are devoid of water (Figure 5a). In these pure methanol systems, the number of H-bonds per solvent molecule is (2 × 1300)/1500 = 1.7. Notably, these H-bonding numbers are in close agreement with bulk solution data, where 3.54 and 1.87 H-bonds per molecule were reported for neat water and methanol, respectively.[93] Thus, our data reveal that the presence of a solvent/vapor interface does not cause a marked reduction in the total number of H-bonds for the

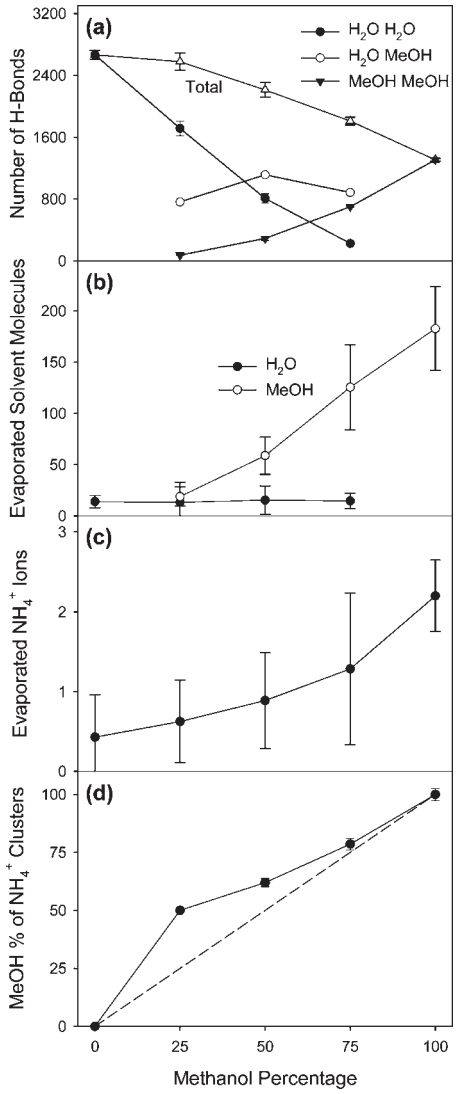

Figure 5. Several droplet parameters are plotted as a function of methanol percentage. (a) Number of different types of H-bonds (water−water, water−methanol, methanol−methanol). Also shown is the total number of H-bonds for each condition. Data were averaged for 3 time points (0, 100, and 200 ps) taken from a single MD run. (b) Number of evaporated solvent molecules after 1 ns. (c) Number of NH_4^+ ejected after 1 ns. (d) Composition of solvated NH_4^+ clusters after ejection. The dashed trend line represents a scenario where the offspring composition matches that of the parent droplet. Data in (b−d) correspond to average values obtained from three to six MD runs. Error bars represent one standard deviation.

droplets, compared to bulk systems. Close inspection of Figures 2 and 3 reveals that surface methanol molecules minimize the loss of H-bonding by pointing their $-CH_3$ group toward the vapor phase.[86] In the case of surface water, one of the O−H bonds points into the vapor phase, such that only a single donor-type interaction is lost. This phenomenon is in line with dangling hydrogens detected by sum frequency spectroscopy[94] and in previous simulations.[60,95]

The reduction in overall H-bonding with increasing methanol concentration diminishes cohesive interactions within the droplets. The resulting destabilization provides the mechanistic basis for the enhanced dynamics of methanol-containing droplets that was noted earlier (Figures 1−3). In addition, the reduced intermolecular contacts have a major effect on the solvent evaporation kinetics (Figure 5b). Only ∼14 solvent molecules evaporate during the 1 ns simulation window from purely aqueous droplets, whereas ∼180 molecules are lost for pure methanol. In the case of equimolar water/methanol mixtures, the evaporation rate of methanol is ca. 4-fold higher than that of water (Figure 5b). Most of these evaporation events correspond to the ejection of single solvent molecules from the droplet surface. Only on rare occasions, two or three H-bonded molecules are ejected together.

The differential evaporation rates of organic/aqueous systems cause a significant water enrichment within mixed ESI nanodroplets. When extrapolating the magnitude of this effect from our 1 ns simulation window to typical lifetimes of larger droplets (μs to ms[33,81]), the time-dependent changes in relative solvent composition can be expected to be dramatic. The existence of this effect has been assumed in several earlier studies.[23,43,96] Recent fluorescence spectroscopic investigations have directly monitored water enrichment within mixed aqueous/organic ESI droplets.[97,98] Analogous phenomena may be operative in the case of ESI supercharging agents.[99,100]

Droplet destabilization due to the loss of H-bonding with increasing methanol concentration also has major implications for the emission of charge carriers. Solvated NH_4^+ get ejected from pure water droplets at a rate of ∼0.5 ions/ns. This rate increases by a factor of 4 for pure methanol (Figure 5c). As noted earlier, NH_4^+ ions are ejected as clusters encompassing roughly ten to twenty solvent molecules. The solvent composition of these small offspring clusters shows a certain degree of methanol enrichment relative to the parent droplet. This effect is most pronounced for a parent droplet methanol content of 25%, where the ejected charged clusters contain 50% methanol (Figure 5d).

Free Energy Profile for Ion Ejection. Further insights into the NH_4^+ dynamics and ejection are obtained when considering the ion free energy G as a function of distance r from the droplet center, where r serves as reaction coordinate. The following considerations are divided into two parts. We will first focus on $G(r)$ within the droplet interior, before considering $G(r)$ in the vicinity of the transition state.

The $P(r)$ ion distribution functions (Figure 4, dotted lines) are a manifestation of the metastable dynamics of NH_4^+ within the droplet. $P(r)dr$ denotes the probability of finding an ion at radial positions in the range r ... $(r + dr)$. We assume that an average potential energy ε can be assigned to an ion that is located at position r. $\varepsilon(r)$ includes all Coulombic and LJ interactions with other ions and solvent molecules. $P(r)$ is given by a Boltzmann distribution[101,102] with

$$P(r)dr = \frac{1}{Z}\exp\left(-\frac{\varepsilon(r)}{k_B T}\right)dW(r) \quad (3)$$

where $dW(r)$ represents the number of energetically equivalent microstates in the range r ... $(r + dr)$. Z is the partition function. With the density of states $D(r) = dW(r)/dr$, eq 3 can be rewritten as

$$P(r)dr = \frac{D(r)}{Z}\exp\left(-\frac{\varepsilon(r)}{k_B T}\right)dr \quad (4)$$

Rearrangements leads to

$$P(r) = \frac{1}{Z}\exp\left(-\frac{G(r)}{k_B T}\right) \quad (5)$$

dx.doi.org/10.1021/ja111492s |J. Am. Chem. Soc. 2011, 133, 9354–9363

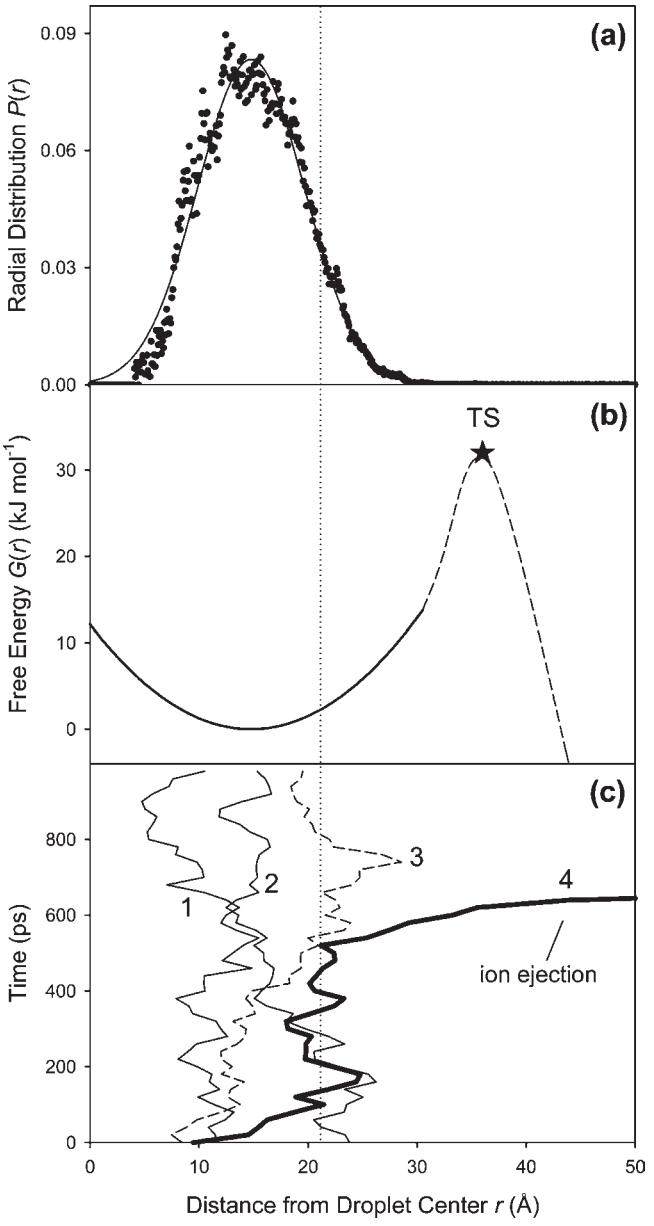

Figure 6. Various aspects of the NH_4^+ dynamics. (a) Radial distribution function $P(r)$ of ammonium ions (taken from Figure 4a), with a fitted Gaussian curve (solid line, eq 8). (b) Free energy profile $G(r)$. The solid line depicts $G(r)$ for ion motion in the droplet interior (eq 10). Also shown (dashed line) is an extension of $G(r)$ toward and beyond the transition state (TS, marked with an asterisk). (c) Radial position of four selected ions (1−4) vs time. Ion 4 gets ejected from the droplet. The vertical dotted line indicates the approximate droplet radius r_0.

where $G(r)$ represents free energy of the ion inside the droplet, with energetic and entropic contributions according to

$$G(r) = \varepsilon(r) - TS(r) \tag{6}$$

The entropy term is given by $S(r) = k_B \ln D(r)$, and the partition function is

$$Z = \int_{r=0}^{\infty} \exp\left(-\frac{G(r)}{k_B T}\right) dr \tag{7}$$

thereby ensuring normalization of $P(r)$ to unity.

Determining $G(r)$ is most straightforward for aqueous droplets with their simple unimodal distribution function (Figure 4a), and hence, we will focus on this particular case. $P(r)$ is well described by a Gaussian function

$$y = a \exp\left(-\frac{1}{2}\left[\frac{r - r_{eq}}{b}\right]^2\right) \tag{8}$$

with $a = 0.0833$, $b = 4.89$ Å, and a quasi-equilibrium position of $r_{eq} = 14.8$ Å (Figure 6a). Equating eqs 5 and 8, and noting that $a = Z^{-1}$ leads to

$$\frac{G(r)}{k_B T} = \frac{1}{2}\left[\frac{r - r_{eq}}{b}\right]^2 \tag{9}$$

Unit conversion from J to J mol^{-1}, using $R = k_B \times N_A$ results in

$$G(r) = \frac{RT}{2}\left[\frac{r - r_{eq}}{b}\right]^2 \tag{10}$$

with the gas constant $R = 8.314$ J K^{-1} mol^{-1}. Equation 10 reveals that the dynamics of NH_4^+ within the nanodroplet interior are governed by a parabolic free energy profile (solid line in Figure 6b).

We will now consider the appearance of $G(r)$ in the transition state region. Ion ejection requires crossing of an activation barrier with $\Delta G^* = G(r_{TS}) - G(r_{eq})$ where r_{TS} denotes the location of the transition state.[33] The original formulation of the IEM assumed that the transition state corresponds to a configuration where a solvated ion has separated and is located a certain distance above the surface of a spherical parent droplet.[33,36] The current work, as well as earlier investigations,[10,11,37,53,54,56,57] has refined this view by noting that ion ejection involves distortion of the parent droplet along with formation of a transient solvent bridge prior to secession (Figures 1−3). Formation of such a protrusion does not always lead to successful ion ejection. Instead, our simulations reveal that configurations as in Figure 1b can also collapse back onto the parent droplet. The transition state r_{TS} reflects the critical protrusion length where the emission probability reaches 0.5.[103] Even without performing a detailed mapping analysis, we can conclude that r_{TS} is close to the linear dimension of a typical protrusion (e.g., Figure 1b,c), measured from the droplet center. For the aqueous droplets considered here, this corresponds to $r_{TS} \approx 35$ Å.

For estimating the activation barrier height, we recall that ion ejection can be treated as a first-order process[33] where the number of bound NH_4^+ ions $N(t)$ decreases according to

$$\frac{N(t)}{N_0} = \exp(-kt) \tag{11}$$

with $N_0 = 11$ and a rate constant k. For aqueous systems with an ejection rate of 0.5 ions/ns (Figure 5c), eq 11 provides a value of $k = 4.7 \times 10^7$ s^{-1}. This corresponds to an activation energy estimate of $\Delta G^* \approx 32$ kJ mol^{-1} (eq 2). In Figure 6b, this barrier at $r_{TS} \approx 35$ Å is indicated by an asterisk. The dashed line in Figure 6b represents a spline extrapolation suggesting a possible shape of the $G(r)$ profile in the vicinity of the transition state. Application of our approach to methanol droplets with their elevated ejection rate of 2 ions/ns (Figure 5c) leads to a lower activation barrier of $\Delta G^* \approx 28$ kJ mol^{-1}. Our estimate of $\Delta G^* \approx 32$ kJ mol^{-1} for aqueous droplets is in quite close agreement with the value of 38 kJ mol^{-1} proposed in the original IEM paper.[33] Barriers on the order of 27 kJ mol^{-1} were

reported in previous MD simulations for ion escape from smaller aqueous droplets.[56,57]

The free energy profile of Figure 6b allows the ion dynamics to be treated as a one-dimensional diffusion process, with escape from a metastable state via thermally activated barrier crossing. This situation is analogous to kinetic phenomena for other complex systems.[102,104,105] Figure 6c illustrates $r(t)$ trajectories of four selected ammonium ions. Ions 1 and 2 undergo Brownian motion[104] relatively close to the bottom of the parabolic $G(r)$ basin for much of the simulation window. Ion 3 initially resides close to the droplet center. It then diffuses toward the liquid/vapor interface, forms a transient surface protrusion around $t = 700$ ps, but ultimately moves back toward the interior. Thus, trajectory 3 represents an unsuccessful ejection event. Ion 4 starts at a radial position around 10 Å. Subsequently, it moves toward the water/vapor interface where it resides for the next 400 ps. At $t \approx 500$ ps, the ion gets entrapped in a surface protrusion, crosses the barrier, and is ejected from the droplet.

CONCLUSIONS

This work examined the behavior of mixed water/methanol nanodroplets close to the Rayleigh limit. The presence of methanol destabilizes the overall droplet structure by reducing the extent of H-bonding. This effect provides the basis for the widespread use of organic cosolvents in ESI-MS, where rapid solvent evaporation and droplet fission are prerequisites for the efficient production of gas phase analyte ions.[6,81]

Nanodroplets containing a relatively low methanol concentration (e.g., 25%, Figure 4b) exhibit significant demixing, with an outer droplet layer that is mostly organic. While not explicitly investigated here, this segregation should favor partitioning of analytes according to their hydrophobicity. Past studies have suggested that surface affinity represents a major determinant of the ESI efficiency, even in homogeneous solvent systems.[6,91,92] In future work, it will be interesting to explore how the presence of an organic outermost droplet layer around an aqueous core affects the analyte behavior.

Our simulations reveal that differential solvent evaporation leads to gradual water enrichment in mixed aqueous/organic droplets. Our findings support the view that late ESI droplets consist almost exclusively of the least volatile solvent component.[23,43,96] However, the situation could be different under nanoESI conditions where the initial droplet radii are much smaller.[29,106] The resulting reduced droplet lifetime and lower number of evaporation/fission cycles may favor the retention of organic solvents in the final droplets.

The diffusive ion dynamics in the interior of aqueous droplets are governed by a parabolic free energy profile. Ion ejection corresponds to thermally activated barrier crossing. Following previous IEM studies,[33,36,37,39] we analyzed ion ejection using transition state theory. Future work is required to determine if the use of a single barrier is adequate. Alternatively, bridged arrangements as in Figures 1−3 might involve additional metastable states. Also, instead of interpreting ion ejection using transition state theory, one might consider the application of Kramers' framework.[104] Kramers' rate expression applies to the diffusive escape from a metastable minimum. Its pre-exponential factor takes into account friction effects, reflecting drag forces experienced by Brownian particles as they move within a viscous medium. Computational and experimental studies on the viscosity dependence of ion ejection could yield additional insights into the properties of the transition barrier.

Earlier studies on large droplets clearly distinguished between Rayleigh fission on one hand, and charge carrier ejection via IEM on the other.[33,36] Figures 1−3 reveal that ion ejection from a nanodroplet morphologically resembles the asymmetric Rayleigh fission of larger droplets.[45−48] Both types of events occur when the droplet charge is close to Q_R.[2,33] One may ask, then, whether a mechanistic distinction between the two processes remains meaningful for the size regime considered here. In other words, can an *"evaporated" ion with its solvent shell* also be interpreted as a (very small) *charged progeny droplet*? Progeny droplets generated during typical Rayleigh fission events contain ∼2% of the parent mass and ∼15% of the charge.[81] These values are close to those observed here, although Rayleigh fission typically involves multiple progeny droplets whereas the ejection of single ions is observed here. The latter difference can be rationalized by considering the very small number (and resulting discrete nature) of charge carriers in our nanodroplets. Losing 1/11 of the droplet charge corresponds to a substantial (9%) reduction, which lowers the driving force for subsequent ion ejection. One interesting aspect for the issue at hand is the observation that ion emission from charged nanodroplets is associated with a major activation barrier (Figure 6b). The presence of such a barrier is a salient IEM feature,[33−37] whereas droplet fission by the Rayleigh mechanism is thought to proceed in a barrier-free fashion.[1,19−21] On the basis of this criterion, it would appear that the ion ejection observed here is more appropriately interpreted as IEM-like field emission, rather than Rayleigh fission. Nonetheless, the dividing line between the two mechanisms becomes somewhat blurred for droplets in the nanoregime, especially when the discussion is based on morphological features. The absence of barrier-free disintegration events in the current simulations may be attributable to the lack of collective shape fluctuations (such as prolate-oblate oscillations) in the initial droplets.[1,19] Additional work will be required to explore the effects of such collective oscillations, which might represent an important determinant for the behavior of real ESI droplets.

It is hoped that future extensions of this study will provide further insights into the behavior of charged solvent droplets under ESI conditions. NH_4^+ ions were considered here because they represent a commonly used solvent additive in ESI-MS. From an analytical perspective, NH_4^+ ejection is of limited interest. However, it seems likely that ESI of small bioorganic species which exist as preformed ions will follow a mechanism similar to that discussed above for NH_4^+. Work to test this prediction is currently in progress. We are also exploring the behavior of much larger species, all the way to intact proteins, where a very different mechanism is expected. Also, the droplets considered here do not contain any counterions. Simulations involving both cations and anions are underway, with the aim of gaining insights into possible ion pairing and cluster formation.[29] The results of those investigations will be reported elsewhere.

ASSOCIATED CONTENT

Supporting Information. Movies of the MD simulation runs of Figures 1−3. This material is available free of charge via the Internet at http://pubs.acs.org.

AUTHOR INFORMATION

Corresponding Author
konerman@uwo.ca

■ ACKNOWLEDGMENT

This work was financially supported by the Natural Sciences and Engineering Research Council of Canada (NSERC), The University of Western Ontario, and the Canada Research Chairs Program. Simulations were carried out using SHARCNET (www.sharcnet.ca).

■ REFERENCES

(1) Rayleigh, L. *Phil. Mag.* **1882**, *14*, 184–186.
(2) Kebarle, P.; Verkerk, U. H. *Mass Spectrom. Rev.* **2009**, *28*, 898–917.
(3) Hogan, C. J.; de la Mora, J. F. *Phys. Chem. Chem. Phys.* **2009**, *11*, 8079–8090.
(4) Cole, R. B. *Electrospray Ionization Mass Spectrometry*; John Wiley & Sons, Inc.: New York, 1997.
(5) Van Berkel, G. J.; Kertesz, V. *Anal. Chem.* **2007**, *79*, 5511–5520.
(6) Cech, N. B.; Enke, C. G. *Mass Spectrom. Rev.* **2001**, *20*, 362–387.
(7) Giglio, E.; Gervais, B.; Rangama, J.; Manil, B.; Huber, B. A. *Phys. Rev. E* **2008**, *77*, 036319.
(8) Feng, X.; Bogan, M. J.; Agnes, G. R. *Anal. Chem.* **2001**, *73*, 4499–4507.
(9) Tang, K.; Smith, R. D. *Int. J. Mass Spectrom.* **1999**, *185/186/187*, 97–105.
(10) Ichiki, K.; Consta, S. *J. Phys. Chem. B* **2006**, *110*, 19168–19175.
(11) Marginean, I.; Znamenskiy, V.; Vertes, A. *J. Phys. Chem. B* **2006**, *110*, 6397–6404.
(12) Storozhev, V. B.; Nikolaev, E. N. *Phil. Mag.* **2004**, *84*, 157–171.
(13) Hogan, C. J.; Carroll, J. A.; Rohrs, H. W.; Biswas, P.; Gross, M. L. *Anal. Chem.* **2009**, *81*, 369–377.
(14) Luedtke, W. D.; Landmann, U.; Chiu, Y.-H.; Levandier, D. J.; Dressler, R. A.; Sok, S.; Gordon, M. S. *J. Phys. Chem. A* **2008**, *112*, 9628–9649.
(15) Labowsky, M. *Rapid Commun. Mass Spectrom.* **2010**, *24*, 3079–3091.
(16) Fenn, J. B. *Angew. Chem., Int. Ed.* **2003**, *42*, 3871–3894.
(17) Pan, P.; McLuckey, S. A. *Anal. Chem.* **2003**, *75*, 1491–1499.
(18) Gu, W.; Heil, P. E.; Choi, H.; Kim, K. *Appl. Phys. Lett.* **2007**, *91*, 064104.
(19) Konermann, L. *J. Am. Soc. Mass Spectrom.* **2009**, *20*, 496–506.
(20) Last, I.; Levy, Y.; Jortner, J. *Proc. Natl. Acad. Sci. U.S.A.* **2002**, *99*, 9107–9112.
(21) Lyalin, A. G.; Obolensky, O. I.; Greiner, W. *Rom. Rep. Phys.* **2007**, *59*, 499–513.
(22) Dole, M.; Mack, L. L.; Hines, R. L.; Mobley, R. C.; Ferguson, L. D.; Alice, M. B. *J. Chem. Phys.* **1968**, *49*, 2240–2249.
(23) Iavarone, A. T.; Williams, E. R. *J. Am. Chem. Soc.* **2003**, *125*, 2319–2327.
(24) de la Mora, F. J. *Anal. Chim. Acta* **2000**, *406*, 93–104.
(25) Felitsyn, N.; Peschke, M.; Kebarle, P. *Int. J. Mass Spectrom. Ion Processes* **2002**, *219*, 39–62.
(26) Nesatyy, V. J.; Suter, M. J.-F. *J. Mass Spectrom.* **2004**, *39*, 93–97.
(27) Kaltashov, I. A.; Mohimen, A. *Anal. Chem.* **2005**, *77*, 5370–5379.
(28) Heck, A. J. R.; Van den Heuvel, R. H. H. *Mass Spectrom. Rev.* **2004**, *23*, 368–389.
(29) Juraschek, R.; Dulcks, T.; Karas, M. *J. Am. Soc. Mass Spectrom.* **1999**, *10*, 300–308.
(30) Pan, J.; Xu, K.; Yang, X.; Choy, W. Y.; Konermann, L. *Anal. Chem.* **2009**, *81*, 5008–5015.
(31) Sun, J.; Kitova, E. N.; Sun, N.; Klassen, J. S. *Anal. Chem.* **2007**, *79*, 8301–8311.
(32) Peschke, M.; Verkerk, U. H.; Kebarle, P. *J. Am. Soc. Mass Spectrom.* **2004**, *15*, 1424–1434.
(33) Iribarne, J. V.; Thomson, B. A. *J. Chem. Phys.* **1976**, *64*, 2287–2294.
(34) Thomson, B. A.; Iribarne, J. V. *J. Chem. Phys.* **1979**, *71*, 4451.
(35) Gamero-Castaño, M.; de la Mora, F. *J. Mass Spectrom.* **2000**, *35*, 790–803.
(36) Tang, L.; Kebarle, P. *Anal. Chem.* **1993**, *65*, 3654–3668.
(37) Labowsky, M.; Fenn, J. B.; Fernandez de la Mora, J. *Anal. Chim. Acta* **2000**, *406*, 105–118.
(38) Loscertales, I. G.; de la Mora, J. F. *J. Chem. Phys.* **1995**, *103*, 5041–5060.
(39) Wang, G.; Cole, R. B. *Anal. Chim. Acta* **2000**, *406*, 53–65.
(40) Spencer, E. A. C.; Ly, T.; Julian, R. K. *Int. J. Mass Spectrom.* **2008**, *270*, 166–172.
(41) Nguyen, S.; Fenn, J. B. *Proc. Natl. Acad. Sci. U.S.A.* **2007**, *104*, 1111–1117.
(42) Fenn, J. B.; Rosell, J.; Meng, C. K. *J. Am. Soc. Mass Spectrom.* **1997**, *8*, 1147–1157.
(43) Samalikova, M.; Grandori, R. *J. Am. Chem. Soc.* **2003**, *125*, 13352–13353.
(44) Smith, J. N.; Flagan, R. C.; Beauchamp, J. L. *J. Phys. Chem. A* **2002**, *106*, 9957–9967.
(45) Gomez, A.; Tang, K. *Phys. Fluids* **1994**, *6*, 404–414.
(46) Duft, D.; Achtzehn, T.; Muller, R.; Huber, B. A.; Leisner, T. *Nature* **2003**, *421*, 128.
(47) Li, D.; Marquez, M.; Xia, Y. *Chem. Phys. Lett.* **2007**, *445*, 271–275.
(48) Nemes, P.; Marginean, I.; Vertes, A. *Anal. Chem.* **2007**, *79*, 3105–3116.
(49) Zweir, T. S. *Science* **2004**, *304*, 1119–1120.
(50) Shin, J.-W.; Hammer, N. I.; Diken, E. G.; Johnson, M. A.; Walters, R. S.; Jaeger, T. D.; Duncan, M. A.; Christie, R. A.; Jordan, K. D. *Science* **2004**, *304*, 1137–1140.
(51) O'Brien, J. T.; Prell, J. S.; Bush, M. F.; Williams, E. R. *J. Am. Chem. Soc.* **2010**, *132*, 8248–8249.
(52) McQuinn, K.; Hof, F.; McIndoe, J. S. *Chem. Commun.* **2007**, *2007*, 4099–4101.
(53) Znamenskiy, V.; Marginean, I.; Vertes, A. *J. Phys. Chem. A* **2003**, *107*, 7406–7412.
(54) Caleman, C.; van der Spoel, D. *Phys. Chem. Chem. Phys.* **2007**, *9*, 5105–5111.
(55) Consta, S. *J. Phys. Chem. B* **2010**, *114*, 5263–5268.
(56) Consta, S. *J. Mol. Struct.:THEOCHEM* **2002**, *591*, 131–140.
(57) Consta, S.; Mainer, K. R.; Novak, W. *J. Chem. Phys.* **2003**, *119*, 10125–10132.
(58) Konermann, L. *J. Phys. Chem. B* **2007**, *111*, 6534–6543.
(59) Patriksson, A.; Marklund, E.; van der Spoel, D. *Biochemistry* **2007**, *46*, 933–945.
(60) Ahadi, E.; Konermann, L. *J. Phys. Chem. B* **2009**, *113*, 7071–7080.
(61) Ahadi, E.; Konermann, L. *J. Am. Chem. Soc.* **2010**, *132*, 11270–11277.
(62) Verlet, L. *Phys. Rev.* **1967**, *159*, 98–103.
(63) Frenkel, D.; Smit, B. *Understanding Molecular Simulations: From Algorithms To Applications*; Academic Press: San Diego, 1996.
(64) Berendsen, H. J. C.; Grigera, J. R.; Straatsma, T. P. *J. Phys. Chem.* **1987**, *91*, 6269–6271.
(65) Haughney, M.; Ferrario, M.; McDonald, I. R. *J. Phys. Chem.* **1987**, *91*, 4934–4940.
(66) Chang, T.-M.; Dang, L. X. *J. Chem. Phys.* **2003**, *118*, 8813–8820.
(67) Forester, T. R.; Smith, W. *J. Comput. Chem.* **1998**, *19*, 102–111.
(68) Nose, S. *Mol. Phys.* **1984**, *52*, 255–268.
(69) Hoover, W. G. *Phys. Rev. A* **1985**, *31*, 1695–1697.
(70) Delhommelle, J.; Millie, P. *Mol. Phys.* **2001**, *99*, 619–625.
(71) Benjamin, I. *J. Chem. Phys.* **1991**, *95*, 3698–3709.
(72) Jungwirth, P.; Tobias, D. J. *J. Phys. Chem. B* **2001**, *105*, 10468–10472.
(73) Wick, C. D.; Dang, L. X. *Chem. Phys. Lett.* **2008**, *458*, 1–5.
(74) Knipping, E. M.; Lakin, M. J.; Foster, K. L.; Jungwirth, P.; Tobias, D. J.; Gerber, R. B.; Dabdub, D.; Finlayson-Pitts, B. J. *Science* **2000**, *288*, 301–306.
(75) Burnham, C. J.; Petersen, M. K.; Day, T. J. F.; Iyengar, S. S.; Voth, G. A. *J. Chem. Phys.* **2006**, *124*, 024327.

(76) Tian, C. S.; Shen, Y. R. *Proc. Natl. Acad. Sci. U. S. A.* **2009**, *106*, 15148–15153.
(77) Petersen, P. B.; Saykally, R. J. *Chem. Phys. Lett.* **2008**, *458*, 255–261.
(78) Douady, J.; Calvo, F.; Spiegelman, F. *J. Chem. Phys.* **2008**, *129*, 154305.
(79) Chandler, D. *Nature* **2005**, *437*, 640–647.
(80) Humphrey, W.; Dalke, A.; Schulten, K. *J. Mol. Graphics* **1996**, *14*, 33–38.
(81) Kebarle, P.; Tang, L. *Anal. Chem.* **1993**, *65*, 972A–986A.
(82) Lide, D. R. *CRC Handbook of Chemistry and Physics*; 82nd ed.; CRC Press: Boca Raton, FL, 2001.
(83) Yuet, P. K.; Blankenschtein, D. *J. Phys. Chem. B* **2010**, *114*, 13786–13795.
(84) Bahadur, R.; Russell, L. M.; Alavi, S. *J. Phys. Chem. B* **2007**, *111*, 11989–11996.
(85) Bahadur, R.; Russel, L. M. *Aerosol Sci. Technol.* **2008**, *42*, 369–376.
(86) Chang, T.-M.; Dang, L. X. *J. Phys. Chem. B* **2005**, *109*, 5759–5765.
(87) Brodskaya, E. N. *Colloid J.* **2001**, *63*, 5–9.
(88) Guo, J. H.; Luo, Y.; Augustsson, A.; Kashtanov, S.; Rubensson, J. E.; Shuh, D. K.; Agren, H.; Nordgren, J. *Phys. Rev. Lett.* **2003**, *91*, 157401.
(89) Dixit, S.; Crain, J.; Poon, W. C. K.; Finney, J. L.; Soper, A. K. *Nature* **2002**, *416*, 829–832.
(90) Allison, S. K.; Fox, J. P.; Hargreaves, R.; Bates, S. P. *Phys. Rev. B* **2005**, *71*, 024201.
(91) Kuprowski, M. C.; Konermann, L. *Anal. Chem.* **2007**, *79*, 2499–2506.
(92) Null, A. P.; Nepomuceno, A. I.; Muddiman, D. C. *Anal. Chem.* **2003**, *75*, 1331–1339.
(93) Hawlicka, E.; Swiatla-Wojcik, D. *Chem. Phys.* **1998**, *232*, 361–369.
(94) Shen, Y. R.; Ostroverkhov, V. *Chem. Rev.* **2006**, *106*, 1140–1154.
(95) Petersen, M. K.; Iyengar, S. S.; Day, T. J. F.; Voth, G. A. *J. Phys. Chem. B* **2004**, *108*, 14804–14806.
(96) Grimm, R. L.; Beauchamp, J. L. *J. Phys. Chem. A* **2010**, *114*, 1411–1419.
(97) Wang, R.; Zenobi, R. *J. Am. Soc. Mass Spectrom.* **2010**, *21*, 378–385.
(98) Zhou, S.; Cook, K. D. *Anal. Chem.* **2000**, *72*, 963–969.
(99) Sterling, H. J.; Daly, M. P.; Feld, G. K.; Thoren, K. L.; Kintzer, A. F.; Krantz, B. A.; Williams, E. R. *J. Am. Soc. Mass Spectrom.* **2010**, *21*, 1762–1774.
(100) Lomeli, S. H.; Peng, I. X.; Yin, S.; Ogorzalek Loo, R. R.; Loo, J. A. *J. Am. Soc. Mass Spectrom.* **2010**, *21*, 127–131.
(101) Dill, K. A.; Bromberg, S. *Molecular Driving Forces*; Garland: New York, 2003.
(102) Konermann, L. *Proteins* **2006**, *65*, 153–163.
(103) Snow, C. D.; Rhee, Y. M.; Pande, V. J. *Biophys. J.* **2006**, *91*, 14–24.
(104) Hanggi, P.; Talkner, P.; Borkovec, M. *Rev. Mod. Pys.* **1990**, *62*, 251–342.
(105) Bieri, O.; Kiefhaber, T. In *Mechanisms of Protein Folding*; Pain, R. H., Ed.; University Press: Oxford, 2000.
(106) Wilm, M.; Mann, M. *Anal. Chem.* **1996**, *68*, 1–8.